JBC Papers in Press. Published on September 13, 2019 as Manuscript RA118.007283
The latest version is at http://www.jbc.org/cgi/doi/10.1074/jbc.RA118.007283

Proteomic mapping by rapamycin-dependent targeting of APEX2 identifies binding partners of VAPB at the inner nuclear membrane

Christina James[1], Marret Müller[1], Martin W. Goldberg[2], Christof Lenz[3,4], Henning Urlaub[3,4] and Ralph H. Kehlenbach[1,*]

[1]Department of Molecular Biology, Faculty of Medicine, GZMB, Georg-August-University Göttingen, Humboldtallee 23, 37073 Göttingen, Germany
[2]School of Biological and Biomedical Sciences, Durham University, Durham, DH1 3LE, UK
[3]Bioanalytics Group, Institute of Clinical Chemistry, University Medical Center Göttingen, Robert-Koch-Straße 40, 37075 Göttingen, Germany
[4]Bioanalytical Mass Spectrometry Group, Max Planck Institute for Biophysical Chemistry, Am Fassberg 11, 37077 Göttingen, Germany

* Corresponding author

Running title: Binding partners of VAPB at the inner nuclear membrane

* to whom correspondence should be addressed:
Tel. +49 551 395950; Fax: +49 551 395960; e-mail: rkehlen@gwdg.de

Keywords: APEX, emerin, nuclear envelope, proteomic proximity mapping, RAPIDS, VAPB, ELYS

VAPB (vesicle-associated membrane protein-associated protein B) is a tail-anchored protein that is present at several contact sites of the endoplasmic reticulum (ER). We now show by immunoelectron microscopy that VAPB also localizes to the inner nuclear membrane (INM). Using a modified APEX2 (enhanced ascorbate peroxidase 2)-approach with rapamycin-dependent targeting of the peroxidase to a protein of interest, we searched for proteins that are in close proximity to VAPB, particularly at the INM. In combination with stable isotope labeling with amino acids in cell culture (SILAC), we confirmed many well-known interaction partners at the level of the ER with a clear distinction between specific and non-specific hits. Furthermore, we identified emerin, TMEM43 and ELYS as potential interaction partners of VAPB at the INM and the nuclear pore complex, respectively.

The family of vesicle-associated membrane protein (VAMP/synaptobrevin) associated proteins (VAPs) includes VAPA and VAPB with described roles in the morphology and the function of the endoplasmic reticulum (ER) and the Golgi apparatus (1,2). VAPB is a tail-anchored protein, i.e. a protein containing a single transmembrane domain close to its C-terminus. Such proteins are typically inserted into the cellular membrane system in a post-translational manner (3,4). In its N-terminal region, VAPB contains a characteristic major sperm protein (MSP) domain. VAPB localizes largely to the ER and its binding to several partner proteins has been shown to mediate the association of the ER with other organelles. The acyl-CoA binding domain protein 5 (ACBD5), for example, interacts with VAPB and is involved in binding peroxisomes to the ER (5), whereas tyrosine phosphatase interacting protein 51 (PTPIP51) and VAPB form an ER-mitochondria tethering complex (6). In the secretory pathway, VAPB interacts with the Yip1-interacting factor homologue YIF1A, e.g. at the level of the ER-Golgi intermediate compartment (7). Furthermore, several oxysterol binding proteins (OSBPs), which play important roles in lipid transport,

interact with VAPB (8) and Kv2 potassium channels form ER-plasmamembrane junctions via interactions with VAPB (9). In total, >100 proteins have been reported to directly or indirectly interact with VAPB and/or the highly similar protein VAPA (10,11) (see also https://thebiogrid.org). A major binding motif, which is found in many VAPB-interacting proteins, is the "two phenylalanines in an acidic tract" (FFAT)-motif (11,12). Typically, the FFAT- (or FFAT-like) motif interacts with the MSP-domain of VAPB. One example for a protein containing the FFAT-motif that binds VAPB is the WD repeat-containing protein WDR44 (13). A mutation in VAPB (P56S) is involved in an autosomal dominant form of amyotrophic lateral sclerosis (ALS) (14) and blocks transport of nucleoporins and emerin, a major protein of the inner nuclear membrane (INM), to the nuclear envelope (15).

Several methods have been developed for the identification of proteins that are in close proximity to each other. They typically introduce biotin into unknown proteins as a tag that can be used for affinity capture with immobilized streptavidin and subsequent analysis by mass-spectrometry (for review see (16,17)). One prominent approach, proximity-dependent biotin identification (BioID), is based on a mutant form of the biotin ligase BirA, which can be fused to a protein of interest (the bait) whose neighboring proteins are to be analyzed (18). The enzyme part of the fusion protein releases reactive biotin, which can modify proteins (the prey) within a small spatial range. One drawback of this method is a rather long reaction time of >15 hours, although a faster method has been described very recently (19). As an alternative to biotin ligase dependent modifications, peroxidase-based methods have been introduced that allow short reaction times in the range of seconds to minutes (20). Ascorbate peroxidase (APEX) is a plant enzyme that generates biotin-phenoxyl radicals from biotin phenol in the presence of H_2O_2. These radicals have a very short half-life and, thus, can modify proteins within a range of ~20 nm, reacting with several amino acids with tyrosine as the primary site of biotinylation (21). Importantly, APEX can be fused to the N- or the C-terminus of proteins and may also reside internally. Furthermore, the enzyme has been shown to be active in several cellular compartments (20,22,23). Recently, APEX2 was introduced, which is far more active than the original enzyme (24). So far, APEX- or APEX2-based methods have mainly been used for the identification of proteins that reside in defined subcellular compartments, e.g. in primary cilia (23) or in the intermembrane space of mitochondria (25). As an alternative to APEX, horseradish peroxidase (HRP) can also be used as an enzyme to initiate the formation of biotin-phenoxyl radicals, and antibody-directed targeting of HRP to proteins of interest was recently described (26).

We previously characterized the post-translational insertion mechanisms of emerin into ER-membranes and analyzed targeting of the protein to the INM (27). For this, we applied a rapamycin-dependent dimerization method to monitor sequestration of a soluble nuclear reporter protein (dGFP-GST-NLS-FKBP12) to mCherry-tagged emerin (mCherry-FRB-emerin) at the INM. In this system, rapamycin binds to its two cognate binding regions, a 12-kDa FK506 binding protein (FKBP12) and an FKBP-rapamycin-binding (FRB)-cassette, promoting rapid interaction of the appropriately tagged proteins (28).

We now combine the APEX2-technology with the rapamycin-dependent dimerization approach. To this end, we target FKBP12-tagged APEX2 to FRB-tagged proteins in a rapamycin-dependent manner. SILAC, followed by quantitative mass spectrometry, then allows the comparison of proteins that get biotinylated by APEX2 in either the absence or the presence of rapamycin. Using this method (rapamycin- and APEX-dependent identification of proteins by SILAC or RAPIDS), we found RMDN3 (PTPIP51), ACBD5, YIF1A, OSBPL9 and other previously known interacting proteins of VAPB. Using a version of APEX2 that accumulates in the nucleus, we identified additional neighboring proteins of VAPB that reside at the nuclear envelope, e.g. emerin, TMEM43, lamins and the nucleoporin ELYS (embryonic large molecule derived from yolk

sac; AHCTF1). We further demonstrate the INM-localization of VAPB by immunoelectron microscopy and confirm the close proximity of endogenous VAPB with several of the newly identified proteins using proximity ligation assays and co-immunoprecipitation experiments.

Results

VAPB resides at the INM

VAPB is typically described as an ER-resident protein, mediating interactions with multiple organelles. In addition, VAPB seems to play a role in the dynamics of the nuclear envelope and the nuclear pore complex. In this context, it was reported to affect transport of emerin to the INM (15). A localization of VAPB itself to the INM, however, has not been demonstrated so far. We therefore investigated the subcellular localization of VAPB in detail. First, we analyzed endogenous VAPB by indirect immunofluorescence using different buffers for the procedure. The specificity of the anti-VAPB antibody was confirmed by siRNA-mediated knockdown (compare Fig. 6). As shown before, VAPB localized to the endoplasmic reticulum (ER), with a clear rim around the nucleus visible in many cells (Fig. 1A). Interestingly, the ratio of the ER- and the nuclear envelope signal varied a lot, depending on the buffer used (compare (i) and (ii)). Similar to the endogenous protein, differently tagged versions of VAPB (mCherry-FRB-VAPB and HA-FRB-VAPB) were also found at the level of the ER and the nuclear envelope (Fig. 1B). We next tested if the nuclear rim could reflect targeting of VAPB not only to the outer, but also to the inner nuclear membrane. For readout, we used our established rapamycin-system (27). As shown before for emerin, the nuclear reporter protein dGFP-GST-NLS-FKBP12 was sequestered to the nuclear rim upon the addition of rapamycin in cells co-expressing mCherry-FRB-VAPB (Fig. 1C). This result suggested that at least a portion of the exogenously expressed VAPB reached the INM. To unequivocally demonstrate INM-localization of endogenous VAPB, we performed immunoelectron microscopy. As shown in Fig. 1D, immunoreactivity was detected at mitochondria, possibly reflecting the interaction of VAPB with PTPIP51. Furthermore, a significant number of gold dots were found at the level of the INM and also in close proximity to nuclear pores. In addition to these morphological studies, we also performed biochemical analyses. Obtaining pure INM-fractions is hardly possible, nevertheless, we subjected cell lysates to an established fractionation protocol (29). As shown in Fig. S1, VAPB was largely recovered in the same fraction as emerin and other proteins of the nuclear envelope, although other membrane proteins are certainly expected in this fraction as well. Together, our results clearly point to a localization of a fraction of the cellular VAPB-pool at the INM. They are in line with a recent study that was published during the review process of this paper, suggesting a role of VAPB in nuclear egress of Herpes Simplex viral particles (30).

APEX2-dependent biotinylation of proteins

A number of membrane proteins exposing binding regions to the cytoplasm have been shown to interact with the ER-form of VAPB (2). A portion of VAPB, however, localizes to the INM and we now set out to devise a method for the identification of neighboring partners of VAPB that allows to focus on either the cytoplasm (where the majority of VAPB is expected) or the nuclear compartment. Our approach is based on the APEX2-method for identification of proximity partners. In a “classic” approach, we first fused APEX2 directly to VAPB (Fig. 2A, left), as done before for many other proteins (9,20-23,25,31-35). HeLa cells were transfected with constructs coding for APEX2-VAPB or, for a control reaction, GFP-APEX2. Fig. 2B shows the subcellular localization of the APEX2-fusion proteins: as expected, GFP-APEX2 is found all over the cell and should promote unspecific biotinylation of many cellular proteins, whereas APEX2-VAPB localizes largely to the ER, very similar to other fusion proteins of VAPB (compare Fig. 1B). Next, the cells were subjected to the biotinylation protocol, including loading of cells with biotin-phenol and a short pulse with H_2O_2. For

analysis, biotinylated proteins were enriched using neutravidin beads and detected by Western-blotting. As shown in Fig. 2C, both fusion proteins were detected at similar levels in total cell lysates and in the protein fractions as bound to the neutravidin beads, indicating self-biotinylation. Furthermore, they led to a similar pattern of biotinylated proteins as detected by streptavidin-HRP. Next, we probed the blots with antibodies against proteins that had previously been identified as interaction partners of VAPB. Indeed, ACBD5 and OSBPL9 were clearly enriched when cells expressed APEX2-VAPB. In the control cells expressing GFP-APEX2, much lower levels of ACBD5 and OSBPL9 were detected (compare lanes 7 and 8). This result shows that the APEX-method is suited for the identification of interaction/proximity partners of VAPB at the level of the ER. We noted, however, that the difference between specific and unspecific biotinylation (i.e. modification in cells expressing APEX2-VAPB versus cells expressing GFP-APEX2) varied a lot, possibly resulting from different transfection efficiencies. We therefore modified our approach in a way that should allow a better control over specific versus unspecific biotinylation and combined APEX2-dependent biotinylation with the protocol for rapamycin-dependent targeting of proteins to a protein of interest (27). For a first proof-of-principle, we constructed a GFP-linked version of APEX2 with the rapamycin-interaction cassette FKBP12 (Fig. 2A, right). Cells were transfected with this construct, together with a construct coding for mCherry-FRB-VAPB. Transfected cells were treated with or without rapamycin and subjected to the biotinylation protocol. Fig. 2B shows the localization of mCherry-FRB-VAPB at the ER and the nuclear envelope and the recruitment of GFP-FKBP12-APEX2 to these sites upon addition of rapamycin. This treatment resulted in a pronounced overlap of the GFP- and the mCherry-signals, suggesting a tight interaction of FKBP12-GFP-APEX2 with mCherry-FRB-VAPB (compare Fig. 1C). As for the "classic" approach, cells were then subjected to the biotinylation protocol and biotinylated proteins were analyzed by Western-blotting. As shown in Fig. 2C, ACBD5 and OSBPL9 were detected as biotinylated proteins (i.e. in the bound fraction) when cells had been treated with the drug, indicating rapamycin-dependent targeting of APEX2 to mCherry-FRB-VAPB and biotinylation of the known VAPB-interaction partners. The levels of proteins that were recovered from the neutravidin beads were as high or higher than those found in the "classic" experiment using APEX2-VAPB as a fusion protein (compare lanes 4 and 8; compare also Fig. 3C). The added advantage of rapamycin-dependent targeting of APEX2 to our protein of interest, however, is twofold: first, a simple, single-parameter-change experiment (+/- rapamycin) can be performed for subsequent analysis of biotinylated proteins by quantitative mass spectrometry and discrimination between specific and unspecific hits. Second, the physical separation of APEX2 from the protein of interest allows an independent subcellular localization of the enzyme and, hence, a control over the population of cellular proteins that are potential targets for biotinylation. This is of particular importance for proteins like VAPB that can engage in interactions with different sets of proteins residing at distinct localizations.

Rapamycin- and APEX-dependent identification of proteins by SILAC (RAPIDS)

Based on the results described above, we decided to use the combined APEX2/rapamycin system for the identification of novel VAPB-proximity partners. The outline for an experiment with a version of APEX2 with the rapamycin-interaction cassette and identification of proteins by SILAC and quantitative mass-spectrometry is depicted in Fig. 3A. Briefly, cells are grown in media containing either light or heavy isotopes of the amino acids lysine and arginine and transfected with plasmids coding for mCherry-FRB-VAPB and FKBP12-GFP-APEX2. The two types of cells ("light" and "heavy") are then treated with or without rapamycin and subjected to the biotinylation procedure. Cellular lysates are combined and biotinylated proteins are enriched by binding to neutravidin beads. Mass-spectrometry of

eluted proteins then allows a direct comparison between plus- (i.e. specific biotinylation close to mCherry-FRB-VAPB) and minus- (i.e. background biotinylation) rapamycin conditions. A quantitative evaluation of heavy and light tryptic fragments of biotinylated proteins should immediately yield proteins that were in close proximity to mCherry-FRB-VAPB in the presence of rapamycin. Fig. S2A shows the controls for H_2O_2-dependent protein biotinylation. Prominent bands that are seen in the absence of H_2O_2 correspond to endogenously biotinylated proteins. Similar transfection efficiencies in the two sets of cells ("light" and "heavy") are controlled in Fig. S2B.

Fig. 3B shows the combined results of two independent experiments, each with forward (i.e. using light and heavy medium for the plus- and minus-rapamycin conditions) and reverse reactions (i.e. with changed conditions, as depicted in Fig. 3A). Proteins that are preferentially biotinylated in the presence of rapamycin in both forward- (X-axis) and reverse-reactions (Y-axis) are expected in the upper left quadrant of the plot. One prominent protein here is VAPB itself, indicating its modification by the APEX2-fusion protein. Many previously known cytoplasmic interaction partners of VAPB were also identified with high levels of significance, including PTPIP51 (RMDN3), YIF1A, WDR44, OSBPL9, OSBPL8 and ACBD5. GAPDH, by contrast, was found in the cloud of proteins that were hardly affected by rapamycin, close to the intersection of the x- and the y-axis. The list of identified proteins is presented in Table S1. Interestingly, the INM-protein emerin was also identified with a high significance. Another potential interaction partner is TMEM43, also known as LUMA, a membrane protein that interacts with emerin at the INM (36) and plays a role in certain forms of muscular dystrophies (37). Its localization is, however, controversial, since it was mainly found in zonula adhaerens and punctum adhaerens plaques in another study (38). Another nuclear protein that was identified is the AT-rich interactive domain-containing protein 4 A (ARID4A). This protein, also known as Rbbp1, is a retinoblastoma-binding protein (39) with functions in chromatin remodeling (40). The significance of the proximity and/or interaction of VAPB and ARID4A remains to be investigated.

Next, we performed Western-blotting to confirm the mass-spectrometry data. As shown in Fig. 3C, high levels of mCherry-FRB-VAPB, ACBD5, OSBPL9 and emerin were detected in the bound fraction when the cells had been treated with rapamycin, confirming rapamycin-dependent biotinylation. For GAPDH, by contrast, very similar levels were observed for rapamycin-treated and non-treated cells. Based on the successful identification of known interaction partners, we termed our approach "RAPID-SILAC" or "RAPIDS" (Rapamycin- and APEX-dependent identification of proteins by SILAC).

RAPIDS using a nuclear version of APEX2

The identification of emerin supported the notion that VAPB can reach the INM (compare Fig. 1), although emerin could also localize to other regions of the cell (41,42). Two parameters of the assay as performed above disfavor the identification of *bona fide* INM-proteins: first, FKBP12-GFP-APEX2 is found all over the cell and may preferentially interact with VAPB that localizes to the ER upon addition of rapamycin. Second, the version of VAPB in this experiment contains a large cytoplasmic mCherry-tag. Although the protein can reach the INM to some extent (Fig. 1C), the efficiency of diffusion of proteins from the ER via the outer nuclear membrane to the INM in general is clearly affected by the size of the cytoplasmic domain (43-47). We therefore modified our approach twofold (Fig. 4A). First, we used a version of APEX2, APEX2-dGFP-NLS-FKBP12, which strongly accumulates in the nucleus of transfected cells as a result of its nuclear localization signal. Hence, biotinylation of nuclear proteins or INM-proteins should be favored. Second, we designed a smaller version of VAPB, HA-FRB-VAPB, which we expect to diffuse more readily across the nuclear pore to the INM than the mCherry-tagged version. As shown in Fig. 4B, APEX2-dGFP-NLS-FKBP12 localized largely in the nucleus in the absence of rapamycin. Upon addition of the drug, the

reporter protein was sequestered to the nuclear envelope, suggesting binding to HA-FRB-VAPB at the INM. We then performed RAPIDS and could show that VAPB (i.e. HA-FRB-VAPB in this experiment) was prominently biotinylated in the presence of rapamycin (Fig. 4C, D). By quantitative proteomics, we identified at least 22 biotinylated proteins that were enriched on the neutravidin beads upon addition of rapamycin to the cells, suggesting their close proximity to HA-FRB-VAPB (Fig. 4C and Table S2). Strikingly, many of the proteins identified are known to reside on the nuclear side of the nuclear envelope. The proximity-candidates fall into three categories: first, proteins of the INM like emerin, the lamina-associated polypeptide 1 (LAP1 or TOR1AIP1, Torsin-1A-interacting protein 1; (48)) and LAP2β (TMPO, thymopoetin; (48,49)). Another protein in this category is TMEM43, which we also found with mCherry-FRB-VAPB as a bait (Fig. 3); second, proteins of the nuclear pore complex (NPC) like Nup153 (50), Tpr (51) and ELYS (AHCTF1; (52)) and third, components of the nuclear lamina like lamin A and lamin B (LMNA, LMNB; (53)). To confirm preferential biotinylation of candidates in the presence of rapamycin, we performed Western-blotting of proteins eluted from the neutravidin beads (Fig. 4D). Essentially all the tested protein showed increased recovery from neutravidin beads upon treatment of cells with rapamycin, including ELYS, lamin A/C, LAP1 (TOR1AIP1), LAP2β (TMPO) and emerin. Together, our results show that RAPIDS allows the identification of known interaction partners of VAPB and, possibly, of novel proximity- and/or interaction partners.

Validation

Proteins identified by RAPIDS could be direct or indirect binding partners of VAPB and occur in biochemically stable complexes or just reside in very close proximity to our protein of interest. As a first step to distinguish between these possibilities, we performed co-immunoprecipitation experiments, combined with a crosslinking approach to stabilize low-affinity interactions. First, we immunoprecipitated endogenous VAPB using a specific antibody and analyzed the precipitate for co-precipitating proteins. As a control, total IgG was used (Fig. 5A). For the established binding partners of VAPB, ACBD5 and OSBPL9, and also for emerin and TMEM43, specific co-precipitation with VAPB was observed when the cells had been treated with the cleavable bi-functional crosslinker dithiobis(succinimidyl propionate) (DSP). For OSBPL9 and TMEM43, co-precipitation above the IgG-background was also seen in the absence of the crosslinker, suggesting tight interactions. To corroborate these findings, we also used HA-FRB-VAPB-overexpressing cells for co-immunoprecipitation experiments, again with and without DSP as a crosslinking reagent. As shown in Fig. 5B, low levels of ACBD5 and OSBPL9 co-precipitated with overexpressed HA-FRB-VAPB. The levels of coprecipitated proteins strongly increased when the cells had been treated with DSP prior to cell lysis (compare lanes 5 and 7). For emerin and TMEM43 and, to some extent, for ELYS, co-precipitation was observed in the cross-linked samples, suggesting that the corresponding complexes exist in intact cells. Very low levels of co-precipitating proteins were observed when the cells had been transfected with a plasmid coding for HA-FRB (lanes 6 and 8). Together, these results show that VAPB indeed interacts with some of the proteins that were identified as proximity partners by RAPIDS. It remains to be investigated whether these interactions are direct or indirect.

Next, we performed proximity ligation assays (PLAs, (54)), which detect interactions (or at least proximity) of endogenous proteins and allow statements about the precise localization of the protein-protein interactions. These assays are based on the decoration of proteins in fixed cells, first with specific primary antibodies and subsequently with oligonucleotide-linked secondary antibodies. If the proteins of interest are in close proximity (i.e. within ~40 nm), subsequent ligation and amplification reactions lead to formation of a fluorescent product that can easily be detected by microscopy. We first analyzed VAPB with respect to its interaction with known binding partners that were also detected by RAPIDS,

namely ACBD5 and OSBPL9. To characterize our antibodies, we performed immunofluorescence analysis. As shown in Fig. S3A and B, ACBD5 co-localized with the peroxisomal marker protein PMP70, and OSBPL9 with the Golgi-marker GM130, indicating the specificity of the ACBD5- and the OSBPL9-antibodies. In PLAs, specific interactions of VAPB were observed with characteristic patterns of dots: for ACBD5 (Figs. S3C, D), dots were found scattered all over the cell, consistent with signals derived from ER-peroxisome interactions. For OSBPL9, the observed dots were largely found in an area corresponding to the Golgi compartment (Figs. S3E, F). The specificity of the signals was supported by single-antibody controls. These results show that our antibodies are suitable for a faithful detection of VAPB-protein interactions. Next, we performed PLAs with antibodies against VAPB and emerin or ELYS (Fig. 6). TMEM43 was not analyzed here due to lack of PLA-suitable antibodies. For emerin, PLA-dots were mostly observed at the nuclear rim, consistent with the major localization of emerin at the INM (Fig. 6A). For ELYS (Fig. 6B), PLA-dots were observed at the nuclear envelope, but also in the nuclear interior. For both proteins, the number of dots decreased significantly when VAPB had been depleted by specific siRNAs as well as in single-antibody-controls, demonstrating the specificity of the PLA. In summary, co-immunoprecipitation experiments and PLA-assays suggest that VAPB indeed forms complexes with proteins of the INM and/or the NPC. Figure 7 depicts the interactome of VAPB, as revealed by our analysis and by previous studies.

Discussion

RAPIDS

The known binding partners of VAPB localize exclusively to the cytoplasm or to cytoplasmic membranes. The INM-localization of VAPB therefore prompted us to search for nuclear proteins that could interact with VAPB or are at least in close proximity to VAPB at the level of the INM or the NPC. For this, affinity-based methods that require an initial cell-lysis step were not very promising, since the lysis buffers must fulfill two conflicting criteria: they must be strong enough to solubilize protein complexes like the nuclear lamina or the NPC, yet maintain the interactions of interest. Indeed, validation of our candidate proteins by co-immunoprecipitation approaches required a careful choice of specific reaction conditions concerning the lysis buffer, the specific antibody and, importantly, the crosslinker used for stabilization of protein-protein interactions. As an alternative, proximity-based approaches like BioID and the APEX-system have the advantage of targeting proteins in their natural environment, the living cells. BioID, in fact, was initially developed to probe the nuclear lamina for interaction partners of lamin A (18). In the last couple of years, APEX-based biotinylation approaches have been used very successfully for the analysis of the interactome of many proteins (9,20-23,25,31-35). With RAPIDS, we now introduce a method that combines APEX2-dependent biotinylation, rapamycin-dependent targeting of the enzyme to proteins of interest, and quantitative proteomics using SILAC. The use of rapamycin to induce rapid targeting of APEX2 to a specific subcellular localization should facilitate the discrimination between proteins that are modified in a specific vs. a nonspecific manner. Furthermore, a careful choice of the tags used for APEX2- (here: +/- NLS) and the protein of interest (here: HA vs. mCherry) may strongly affect the spectrum of identified proteins. This is of particular importance for proteins of the INM, where the size and the nature of the tag may affect efficient targeting of proteins to their final destination. In general, the approach to physically separate the APEX2-enzyme from the protein of interest offers a tight control over the cellular proteins that are potential targets for biotinylation. This is a clear advantage for proteins like VAPB that can engage in interactions at different intracellular contact sites. Notably, a similar targeting approach using the rapamycin analogue AP21967 as a dimerizing agent was very recently described (55). In 2C-BioID, the authors used the rapamycin analogue AP21967 to initiate dimerization of a biotin-protein

ligase and a protein of interest to analyze the interactomes of LAP2β and lamins A and C as a proof of principle.

The feasibility of RAPIDS was demonstrated by the identification of many of the previously known binding partners of VAPB (Fig. 3). Furthermore, we identified several novel nuclear proximity partners of VAPB, consistent with the INM-localization of the protein. For this, usage of our nuclear version of APEX2 was important, as it favors the biotinylation of nuclear proteins. Fig. 7 summarizes our findings and also indicates some of the proteins that had previously been identified as binding partners of VAPB. Together, RAPIDS is a versatile method for the identification of proteins that are in close proximity to a protein of interest. This modification of the classic APEX-approach should be applicable to proteins residing at different subcellular localizations.

VAPB at the INM

To our knowledge, a nuclear localization of VAPB itself has not been documented so far, except in a very recent publication (30). Using our rapamycin-dependent dimerization assay as well as immunoelectron microscopy, we now unequivocally show that VAPB can indeed reach the INM and can also be detected in close proximity to NPCs (Fig. 1). At this point, we cannot say with certainty, which percentage of the entire cellular pool of endogenous VAPB resides at the INM. In immunofluorescence, the ratio of the nuclear envelope- and the ER-signal of VAPB is affected by the buffer conditions (Fig. 1A). In immunoelectron microscopy (Fig. 1D), epitope masking is a general issue and could affect nuclear and cytoplasmic immunoreactivity of VAPB differently. Hence, other, more quantitative methods are required for an accurate determination of VAPB-levels at different localizations within the cell.

VAPB has been described as a protein that localizes to ER-contact sites (2). Using RAPIDS under conditions that should favor the identification of cytoplasmic binding/proximity partners (i.e. with mCherry-FRB-VAPB and FKBP12-GFP-APEX2; Figs. 2 and 3), we found many of the previously known interaction partners of VAPB, including oxysterol binding proteins, PTPIP51 and ACBD5. Most of the identified proteins associate with membranes and many of them localize to the ER (see Table S1), consistent with the major localization of mCherry-FRB-VAPB. Nevertheless, we also identified emerin as a mainly nuclear protein using this approach, in agreement with the observation that mCherry-FRB-VAPB can reach the INM (Fig. 1C). A different picture emerged when we used FRB-VAPB with an HA-tag at the N-terminal end instead of an mCherry-tag and APEX2-dGFP-NLS-FKBP12 as a nuclear version of the biotinylating enzyme (Fig. 4 and Table S2). Under this condition, we identified significantly more nuclear proteins, including emerin and other membrane proteins of the INM, several nucleoporins and components of the nuclear lamina. This result is consistent with the observation that the efficiency of translocation of proteins from the outer to the inner nuclear membrane inversely correlates with the size of the cytoplasmic/nuclear region of the protein (43-47). Since the HA-tag is significantly smaller than the mCherry-tag, a larger proportion of the overexpressed protein is expected to reach the INM via passive diffusion (45), where, upon rapamycin treatment, the nuclear version of APEX2 can then initiate efficient biotinylation of neighboring proteins.

Importantly, interaction of endogenous VAPB or overexpressed VAPB with emerin and TMEM43 could be confirmed by co-immunoprecipitation experiments, where the novel binding partners behaved very similar to the established binding partners ACBD5 and OSBPL9 (Fig. 5). Interestingly, co-precipitation of TMEM43 with emerin has been described previously (36). For VAPB/emerin and VAPB/ELYS we also confirmed a close proximity *in situ*, using PLA-assays (Fig. 6). For emerin, PLA-dots were largely restricted to the nuclear envelope, consistent with the predominant localization of the protein. ELYS is a nucleoporin that can also localize to the nuclear interior in interphase cells (52) and plays a role in early steps of post-mitotic NPC-assembly (56,57). Hence, a role of VAPB in this process could be

envisaged. ELYS has previously been suggested to interact directly with VAPB based on an FFAT-like motif in its sequence (2,10). In our PLAs, we also observed intranuclear dots, suggesting that not only ELYS, but also VAPB might reside in the nucleoplasm. This seems counterintuitive, since VAPB is a membrane protein. Being a tail-anchored protein, however, a soluble pool of it must exist and a fraction could even reach the nuclear interior. At this point, we can only speculate about the functional significance of INM-localization of VAPB. VAPB has been implicated in the transport of emerin and nucleoporins to the INM and the NPC, respectively (15).

In summary, our findings suggest that the interaction repertoire of VAPB is even larger than previously thought. VAPB not only serves as a bridging factor at multiple contact sites of the ER with mitochondria, peroxisomes, the Golgi apparatus and the plasma membrane, but also localizes to the INM, where it may contact several nucleoporins, integral membrane proteins and components of the nuclear lamina.

Experimental procedures

Plasmids

Standard procedures were used for cloning and the obtained constructs were confirmed by sequencing. To obtain pcDNA3-FKBP12-GFP-APEX2, the FKBP12 coding sequence was originally derived from pcDNA3-FKBP12 (27,58) using primers G1562 and G1563 and cloned into pcDNA3-Connexin43-GFP-APEX2 (Addgene plasmid #49385) through AflII and BamHI, thereby replacing the Connexin43 coding sequence (oligonucleotides are listed in Table S3). For APEX2-dGFP-NLS-FKBP12, the APEX2 coding sequence was amplified by PCR using pcDNA3-Connexin43-GFP-APEX2 as a template and primers G1573 and G1571. The PCR product was cloned into a pEGFP-C1 derivative encoding dGFP-cNLS-FKBP12 through BcuI. For pmCherry-FRB-VAPB, the VAPB coding sequence was amplified by PCR using primers G1390 and G1386 and pCAN-myc-VAPB (59) as a template. The PCR product was cloned into a pmCherry-C1 derivative coding for mCherry-FRB through KpnI and BamHI.

For pEF-HA-FRB-VAPB, the FRB coding sequence (as above) from mCherry-FRB was first inserted into a modified pEF-HA vector (60) via NcoI and EcoRI, generating pEF-HA-FRB. The VAPB coding sequence was amplified by PCR using primers G1512 and G1511 and pCAN-myc-VAPB (59) as a template. The PCR product was then inserted into pEF-HA-FRB plasmid through EcoRI and SpeI. To obtain pEGFP-APEX2, APEX2 was amplified from pcDNA3-FKBP12-GFP-APEX2 using primers G1854 and G1855 and cloned into pEGFP-C1 through EcoR1 and BamH1. For APEX2-VAPB, VAPB was amplified from pmCherry-FRB-VAPB using primers G1512 and G1386 and cloned via EcoR1 and BamH1 into pAPEX2-C1, which had been generated by exchanging the mCherry sequence of pmCherry-C1 for that of APEX2.

Cell culture and transfection

HeLa P4 cells (61) were obtained from the NIH AIDS Reagent Program. Cells were cultivated in DMEM (Life technologies, Carlsbad, CA, USA) supplemented with 10% (v/v) FBS (Life technologies, Carlsbad, CA, USA), 100 U ml^{-1} penicillin, 100 µg ml^{-1} streptomycin and 2 mM L-glutamine (Life technologies, Carlsbad, CA, USA) under 5% CO_2 at 37°C. They were tested regularly for contamination by mycoplasma.

For SILAC, cells were grown in medium containing heavy or light isotopes of arginine and lysine. For this purpose, DMEM (high glucose) lacking glutamine, lysine and arginine (Thermo Fisher Scientific, Waltham, MA, USA) was supplemented with 10% (v/v) dialyzed FBS (Life technologies, Carlsbad, CA, USA), 6 mM L-glutamine (Life technologies), 100 U ml^{-1} penicillin and 100 µg ml^{-1} streptomycin. To obtain SILAC media with heavy and light isotopes, either 0.4 mM $^{13}C_6{}^{15}N_2$-L-lysine (Silantes, Munich, Germany) and 0.2 mM $^{13}C_6{}^{15}N_4$-L-arginine (Silantes, Munich, Germany) or 0.4 mM $^{12}C_6{}^{14}N_2$-L-lysine (Sigma-Aldrich, St. Louis, MO, USA) and 0.2 mM $^{12}C_6{}^{14}N_4$-L-arginine (Sigma-Aldrich, St. Louis, MO, USA) were added,

respectively. To ensure sufficient incorporation of heavy amino acids, cells were passaged five to seven times in SILAC medium before the biotinylation experiment, and the incorporation rate was confirmed to be ≥97% by mass spectrometry.

Transfections were performed according to the calcium phosphate method (62). Briefly, the respective plasmids were mixed with 250 mM $CaCl_2$. After the addition of the same amount of HEPES buffer (50 mM HEPES, pH 6.98, 250 mM NaCl, 1.5 mM $NaHPO_4$) and 20 min incubation at room temperature, the mixture was added to the cells, which were then grown as above.

siRNA mediated knockdown of VAPB was carried out using Lipofectamine RNAiMAX (Thermo Fisher Scientific, Waltham, MA, USA) following the protocol of the manufacturer. VAPB siRNA (GCUCUUGGCUCUGGUGGUUUU, AAAACCACCAGAGCCAAGAGC; Sigma), and ON-Target plus non-targeting siRNA (Dharmacon, Lafayette, CO, USA, D-001810-01-50) were used at a final concentration of 100 nM.

Rapamycin-dependent biotinylation assay

HeLa P4 cells were grown in 10 cm dishes in SILAC medium as described above. Two sets of cells (in "light" or "heavy" medium) were transfected with pmCherry-FRB-VAPB and pcDNA3-FKBP12-GFP-APEX2 or pEF-HA-FRB-VAPB and pAPEX2-dGFP-NLS-FKBP12, using the same transfection mix to ensure similar expression levels, and grown to confluency. Cells were then incubated for 30 min with 500 µM biotin-phenol (Iris Biotech, Marktredwitz, Germany), with or without 200 nM rapamycin (Sigma Aldrich, St. Louis, MO, USA). For each experiment, forward and reverse reactions were performed. For forward reactions, cells grown in "light'' SILAC medium were treated with rapamycin and cells grown in "heavy" SILAC medium were not. For reverse reactions, this labeling scheme was switched. After incubation with biotin-phenol and rapamycin, 1 mM H_2O_2 was added at room temperature. After 1 min, the medium was aspirated and cells were washed twice with quenching buffer (5 mM Trolox, 10 mM NaN_3, 10 mM sodium ascorbate in PBS) and once with PBS. Cells used for fluorescence microscopy were fixed immediately.

For Western blot and SILAC analyses, cells from each dish were lysed with 1 ml RIPA buffer (50 mM Tris, pH 7.4, 5 mM Trolox, 0.5% (w/v) sodium deoxycholate, 150 mM NaCl, 0.1% (w/v) sodium dodecyl sulfate (SDS), 1% (v/v) Triton X-100, 1 mM phenylmethane sulfonyl fluoride (PMSF), 10 mM NaN_3, 10 mM sodium ascorbate, 1 µg ml^{-1} aprotinin, 1 µg ml^{-1} leupeptin and 1 µg ml^{-1} pepstatin). The cell lysate was incubated for 5 min on ice and centrifuged for 10 min at 16,000 g and 4°C. The cleared cell lysate was used to enrich biotinylated proteins with neutravidin beads (Thermo Fisher Scientific, Waltham, MA, USA). For mass spectrometry, cell lysates derived from three 10 cm dishes were pooled, the protein concentration of the cell lysates was determined using the Pierce 660 nm Protein Assay (Thermo Fisher Scientific, Waltham, MA, USA) and equal protein amounts of samples treated with or without rapamycin were mixed prior to addition to neutravidin beads. For Western blot analyses, the samples were kept separately. For each forward or reverse experiment, six batches of 130 µl neutravidin beads were incubated with 1ml cell lysate overnight at 4°C on a rotor. The beads were washed once with washing buffer 1 (50 mM HEPES (pH 7.4), 0.1% (w/v) sodium deoxycholate, 1% (v/v) Triton X-100, 500 mM NaCl, 1 mM ethylenediaminetetraacetic acid (EDTA), once with washing buffer 2 (50 mM Tris (pH 8.0), 250 mM LiCl, 0.5% (v/v) Nonidet P-40, 0.5% (w/v) sodium deoxycholate, 1 mM EDTA) and twice with washing buffer 3 (50 mM Tris (pH 7.4) and 50 mM NaCl). For each washing step, the beads were incubated for 8 min at 4°C on a rotor. After the last washing step, the buffer was removed and bound proteins were eluted from the beads by incubation for 5 min at 95°C with 90 µl SDS sample buffer (4% (w/v) SDS, 125 mM Tris pH 6.8, 10% (v/v) glycerol, 0.02% (v/v) bromophenol blue, 10% (v/v) β-mercaptoethanol) supplemented with 5 mM desthiobiotin (Sigma-Aldrich, St. Louis, MO, USA). To increase the protein concentration,

three batches of beads were consecutively eluted in the same buffer.

Mass spectrometric analyses

Samples were separated on 4-12% NuPAGE Novex Bis-Tris Minigels (Invitrogen, Carlsbad, California). Gels were stained with Coomassie Blue, and each lane sliced into 11-12 equidistant bands. After washing, gel slices were reduced with dithiothreitol (DTT), alkylated with 2-iodoacetamide and digested with trypsin (sequencing grade, Promega, Madison Wisconsin) overnight. The resulting peptide mixtures were then extracted, dried in a SpeedVac, reconstituted in 2% acetonitrile/0.1% formic acid/ (v/v) and analyzed by nanoLC-MS/MS on a hybrid quadrupole/orbitrap mass spectrometer (Q Exactive, Thermo Fisher Scientific, Dreieich, Germany) as described previously (63). Raw data were processed using MaxQuant Software version 1.5.7.4 (Max Planck Institute for Biochemistry, Martinsried, Germany). Proteins were identified against the human reference proteome (v2017.02, 92.927 protein entries) along with a set of common lab contaminants. The search was performed with trypsine (excluding proline-proximal cleavage sites) as enzyme and iodoacetamide as cysteine blocking agent. Up to two missed tryptic cleavages were allowed for, as well as methionine oxidation and protein N-terminal acetylation variable modifications. Instrument type 'Orbitrap' was selected to adjust for MS acquisition specifics. Following an initial internal recalibration, this translated into an MS mass tolerance of 4.5 ppm and an MS/MS mass tolerance of 20 ppm. Protein and peptide results lists were thresholded at False Discovery Rates (FDR) of 0.01, using a forward-and-reverse decoy database approach. The Arginine R10 and Lysine K8 labels including the 'Re-quantify' option were specified for relative protein quantitation. Perseus Software version 1.5.6.0 (Max Planck Institute for Biochemistry, Martinsried, Germany) was used for statistical evaluation of relative protein quantitation values from the MaxQuant Software results and a two-sided Significance B test (64) was performed using normalized $\log_2$ ratios. For the analysis, a Benjamini-Hochberg correction was applied and a threshold value of 0.05 was chosen. Mass spectrometry experiments were performed twice, each with two biological and two technical replicates.

Data availability

The MS proteomics data have been deposited to the ProteomeXchange Consortium via the PRIDE (65) partner repository with the dataset identifier PXD012157 (username: reviewer27517@ebi.ac.uk; password: LrJXmV8h)

Western blot analyses

Western blotting was performed according to standard methods using HRP-coupled secondary antibodies. To detect biotinylated proteins, they were separated by SDS-PAGE using 4-12% NuPAGE Novex Bis-Tris Minigels (Invitrogen, Carlsbad, California). After transfer to nitrocellulose, the membranes were incubated in blocking buffer (3% BSA in TBS-T (24.8 mM Tris, pH 7.4, 137 mM NaCl, 2.7 mM KCl, 1% (v/v) Tween 20)) overnight at 4°C. Incubation with streptavidin-HRP (Jackson ImmunoResearch Laboratories, West Grove, PA, USA; diluted 1:5,000-1:40,000 in blocking buffer) for 1 h at room temperature was followed by three washing steps with TBS-T. For detection of proteins, Immobilon Western Chemiluminescent HRP Substrate (Millipore, Burlington, MA, USA) and a luminescent image analyzer (LAS-3000; Fuji, Tokyo, Japan) were used. Signal intensities were measured using Image Studio Lite (Ver. 5.2). Two-way analysis of variance (ANOVA) followed by Bonferroni post-test was used for statistical analysis and a confidence interval of 95% was set. Primary and secondary antibodies are listed in Table S4.

Immunofluorescence and microscopy

For fluorescence microscopy, cells were grown on coverslips and fixed with 4% (v/v) para formaldehyde. Cells expressing fluorescently labeled proteins were mounted directly with MOWIOL supplemented with 1 µg/ml DAPI. For immunofluorescence, fixed cells were permeabilized with 0.5% (v/v) Triton X-100 in PBS for 5 min at room temperature and

blocked with 3% (w/v) BSA in PBS for 20 min at room temperature. Staining was performed for 1 h at room temperature using appropriate primary antibodies and fluorescently labeled secondary antibodies (Table S4), which were diluted in 3% BSA in PBS. Afterwards, cells were embedded in MOWIOL-DAPI.
Microscopic analysis was performed using an LSM510 Confocal laser scanning microscope using a 63X /1.4 oil immersion lens (Zeiss, Oberkochen, Germany).

Electron microscopy
For immunoelectron microscopy, HeLa cells were fixed with 2% paraformaldehyde, 0.2% glutaraldehyde in PHEM buffer (60 mM Pipes, 25 mM Hepes, 2 mM $MgCl_2$, 10 mM EGTA, pH 6.9) for 1 h, washed with PHEM, and scraped off. Cells were pelleted (200 x g, 2 min) and resuspended in 0.1% glycine in PBS, pelleted (400 x g, 2 min), resuspended in 0.1% glycine in PBS (15 min), pelleted (400 x g, 2 min), resuspended in 1% gelatin (Dr. Oetker) at 37°C for 10 min, pelleted (400 x g, 2 min), resuspended in 10% gelatin for 10 min at 37°C, then replaced on ice. Pellets were immersed in 15% PVP (polyvinylpyrrolidone, 10 kDa, Sigma), 1.7 M sucrose in PBS overnight, then mounted and frozen in liquid nitrogen and sectioned on a cryo-ultramicrotome (Leica UC6 with FC6). Cryosections were thawed and placed at 37°C, washed in 0.1% bovine serum albumin (BSA, Sigma) in PBS, then 1% BSA in PBS for 3 min, followed by overnight incubation with undiluted primary antibody (mouse anti-VAPB mouse, Proteintech), washed in PBS, incubated with 10 nm colloidal gold-anti-mouse antibody (BBI solutions). Grids were washed in PBS, transferred to 1% glutaraldehyde in PBS (5 min), washed in H_2O, and embedded in 2% methyl cellulose containing 0.4% uranyl acetate (Agar Scientific). Imaging was done using a Hitachi H7600 TEM at 100 kV.

Cross-linking and co-immunoprecipitation
$2x10^6$ Hela P4 cells per 10 cm dish were transfected with plasmids coding for HA-FRB-VAPB or HA-FRB. After 24 hours, the cells were washed twice with cold PBS containing 0.1 mM $CaCl_2$ and 1 mM $MgCl_2$ and incubated with DSP (Dithiobis (succinimidyl propionate), Thermo Scientific) at a final concentration of 1 mM in DMSO for two hours on ice. For control reactions, DMSO alone was used. DSP was quenched by the addition of 20 mM Tris-HCl pH 7.4 for 15 min. The cells were then washed twice with cold PBS and lysed with 1 ml lysis buffer (0.5% Na-deoxycholate, 50 mM Tris-HCl pH 7.4, 150 mM NaCl, 0.25% SDS, 0.5% Triton X-100 with complete protease inhibitor cocktail (Roche)) for 30 min on ice. To reduce viscosity, the lysate was passed through a 27Gx3/4" needle and then centrifuged at 15,000g for 20 min at 4°C. For immunoprecipitation, 25 µl anti-HA-agarose beads (Sigma A2095) were washed with washing buffer (10 mM Hepes, 150 mM NaCl, 1 mM EGTA, 0.1 mM $MgCl_2$, 0.1% Triton X-100 and complete protease inhibitor cocktail). The lysate from $24x10^6$ cells was added to the beads and rotated for three hours at 4°C. The beads were then washed four times with washing buffer and proteins were eluted with sample buffer containing 50 mM DTT. For immunoprecipitation of endogenous protein complexes, 4 µg of rabbit-anti-VAPB, rabbit-anti-ELYS or IgG as a control were immobilized on 40 µl Protein A sepharose 4 Fast Flow beads (GE Healthcare) for three hours and incubated with lysates from $24x10^6$ cells that had or had not been subjected to cross-linking as described above.

Proximity Ligation Assay (PLA)
HeLa cells were seeded at a density of 40,000 cells/well in 24-well plates. After 48 hours, cells were fixed with 4% paraformaldehyde and permeabilized with 0.05% (v/v) Triton X-100. PLA assays were performed using the Duolink In Situ PLA kit (Sigma Aldrich, St. Louis, MO, USA, DUO 9200). Cells were blocked and incubated with mouse anti-VAPB and rabbit anti-emerin, rabbit anti-ELYS, rabbit anti-ACBD5 or rabbit anti-OSBPL9, respectively (see Table S4 for antibodies). After ligation and amplification using the corresponding PLA probes, the cells were counterstained for VAPB and mounted using Duolink mounting medium with DAPI. Images were acquired on an LSM510 Confocal laser

scanning microscope using a 63X /1.4 oil immersion lens. 450 cells over three independent experiments were analyzed for PLA interaction using CellProfiler 2.2 (66). One-way analysis of variance (ANOVA) followed by Bonferroni post-test was used for statistical analysis and a confidence interval of 95% was set.

Acknowledgements
The authors would like to thank Thierry Wasselin and Christiane Spillner (University Medical Center Göttingen, Germany) and Christine Richardson (School of Biological and Biomedical Sciences, Durham University, UK) for expert technical assistance, Drs. Eric Schirmer (Edinburgh), Nica Borgese (Milan, Italy) and Sima Lev (Rehovot, Israel) for valuable reagents and Dr. Eric Arakel (Göttingen) for advice. The work was funded by grants from the DFG to RHK and HU (SFB1190).

Conflict of Interest
The authors declare that they have no conflicts of interest with the contents of this article.

References

1. Lev, S., Ben Halevy, D., Peretti, D., and Dahan, N. (2008) The VAP protein family: from cellular functions to motor neuron disease. *Trends Cell Biol* **18**, 282-290
2. Murphy, S. E., and Levine, T. P. (2016) VAP, a Versatile Access Point for the Endoplasmic Reticulum: Review and analysis of FFAT-like motifs in the VAPome. *Biochim Biophys Acta* **1861**, 952-961
3. Casson, J., McKenna, M., Hassdenteufel, S., Aviram, N., Zimmerman, R., and High, S. (2017) Multiple pathways facilitate the biogenesis of mammalian tail-anchored proteins. *J Cell Sci* **130**, 3851-3861
4. Kutay, U., Hartmann, E., and Rapoport, T. A. (1993) A class of membrane proteins with a C-terminal anchor. *Trends Cell Biol.* **3**, 72-75.
5. Costello, J. L., Castro, I. G., Hacker, C., Schrader, T. A., Metz, J., Zeuschner, D., Azadi, A. S., Godinho, L. F., Costina, V., Findeisen, P., Manner, A., Islinger, M., and Schrader, M. (2017) ACBD5 and VAPB mediate membrane associations between peroxisomes and the ER. *J Cell Biol* **216**, 331-342
6. Stoica, R., De Vos, K. J., Paillusson, S., Mueller, S., Sancho, R. M., Lau, K. F., Vizcay-Barrena, G., Lin, W. L., Xu, Y. F., Lewis, J., Dickson, D. W., Petrucelli, L., Mitchell, J. C., Shaw, C. E., and Miller, C. C. (2014) ER-mitochondria associations are regulated by the VAPB-PTPIP51 interaction and are disrupted by ALS/FTD-associated TDP-43. *Nat Commun* **5**, 3996
7. Kuijpers, M., Yu, K. L., Teuling, E., Akhmanova, A., Jaarsma, D., and Hoogenraad, C. C. (2013) The ALS8 protein VAPB interacts with the ER-Golgi recycling protein YIF1A and regulates membrane delivery into dendrites. *EMBO J* **32**, 2056-2072
8. Moustaqim-Barrette, A., Lin, Y. Q., Pradhan, S., Neely, G. G., Bellen, H. J., and Tsuda, H. (2014) The amyotrophic lateral sclerosis 8 protein, VAP, is required for ER protein quality control. *Hum Mol Genet* **23**, 1975-1989
9. Johnson, B., Leek, A. N., Sole, L., Maverick, E. E., Levine, T. P., and Tamkun, M. M. (2018) Kv2 potassium channels form endoplasmic reticulum/plasma membrane junctions via interaction with VAPA and VAPB. *Proc Natl Acad Sci U S A* **115**, E7331-E7340
10. Huttlin, E. L., Ting, L., Bruckner, R. J., Gebreab, F., Gygi, M. P., Szpyt, J., Tam, S., Zarraga, G., Colby, G., Baltier, K., Dong, R., Guarani, V., Vaites, L. P., Ordureau, A., Rad, R., Erickson, B. K., Wuhr, M., Chick, J., Zhai, B., Kolippakkam, D., Mintseris, J., Obar, R. A., Harris, T., Artavanis-Tsakonas, S., Sowa, M. E., De Camilli, P., Paulo, J. A., Harper, J. W., and Gygi, S. P. (2015) The BioPlex Network: A Systematic Exploration of the Human Interactome. *Cell* **162**, 425-440
11. Murphy, R., and Wente, S. R. (1996) An RNA-export mediator with an essential nuclear export signal. *Nature* **383**, 357-360
12. Loewen, C. J., Roy, A., and Levine, T. P. (2003) A conserved ER targeting motif in three families of lipid binding proteins and in Opi1p binds VAP. *EMBO J* **22**, 2025-2035
13. Baron, Y., Pedrioli, P. G., Tyagi, K., Johnson, C., Wood, N. T., Fountaine, D., Wightman, M., and Alexandru, G. (2014) VAPB/ALS8 interacts with FFAT-like proteins including the p97 cofactor FAF1 and the ASNA1 ATPase. *BMC Biol* **12**, 39
14. Nishimura, A. L., Mitne-Neto, M., Silva, H. C., Richieri-Costa, A., Middleton, S., Cascio, D., Kok, F., Oliveira, J. R., Gillingwater, T., Webb, J., Skehel, P., and Zatz, M. (2004) A mutation in the vesicle-trafficking protein VAPB causes late-onset spinal muscular atrophy and amyotrophic lateral sclerosis. *Am J Hum Genet* **75**, 822-831
15. Tran, D., Chalhoub, A., Schooley, A., Zhang, W., and Ngsee, J. K. (2012) A mutation in VAPB that causes amyotrophic lateral sclerosis also causes a nuclear envelope defect. *J Cell Sci* **125**, 2831-2836
16. Gingras, A. C., Abe, K. T., and Raught, B. (2018) Getting to know the neighborhood: using proximity-dependent biotinylation to characterize protein complexes and map organelles. *Curr Opin Chem Biol* **48**, 44-54

17. Kim, D. I., and Roux, K. J. (2016) Filling the Void: Proximity-Based Labeling of Proteins in Living Cells. *Trends Cell Biol* **26**, 804-817
18. Roux, K. J., Kim, D. I., Raida, M., and Burke, B. (2012) A promiscuous biotin ligase fusion protein identifies proximal and interacting proteins in mammalian cells. *J Cell Biol* **196**, 801-810
19. Branon, T. C., Bosch, J. A., Sanchez, A. D., Udeshi, N. D., Svinkina, T., Carr, S. A., Feldman, J. L., Perrimon, N., and Ting, A. Y. (2018) Efficient proximity labeling in living cells and organisms with TurboID. *Nat Biotechnol* **36**, 880-887
20. Rhee, H. W., Zou, P., Udeshi, N. D., Martell, J. D., Mootha, V. K., Carr, S. A., and Ting, A. Y. (2013) Proteomic mapping of mitochondria in living cells via spatially restricted enzymatic tagging. *Science* **339**, 1328-1331
21. Udeshi, N. D., Pedram, K., Svinkina, T., Fereshetian, S., Myers, S. A., Aygun, O., Krug, K., Clauser, K., Ryan, D., Ast, T., Mootha, V. K., Ting, A. Y., and Carr, S. A. (2017) Antibodies to biotin enable large-scale detection of biotinylation sites on proteins. *Nat Methods* **14**, 1167-1170
22. Lobingier, B. T., Huttenhain, R., Eichel, K., Miller, K. B., Ting, A. Y., von Zastrow, M., and Krogan, N. J. (2017) An Approach to Spatiotemporally Resolve Protein Interaction Networks in Living Cells. *Cell* **169**, 350-360 e312
23. Mick, D. U., Rodrigues, R. B., Leib, R. D., Adams, C. M., Chien, A. S., Gygi, S. P., and Nachury, M. V. (2015) Proteomics of primary cilia by proximity labeling. *Dev Cell* **35**, 497-512
24. Lam, S. S., Martell, J. D., Kamer, K. J., Deerinck, T. J., Ellisman, M. H., Mootha, V. K., and Ting, A. Y. (2015) Directed evolution of APEX2 for electron microscopy and proximity labeling. *Nat Methods* **12**, 51-54
25. Hung, V., Zou, P., Rhee, H. W., Udeshi, N. D., Cracan, V., Svinkina, T., Carr, S. A., Mootha, V. K., and Ting, A. Y. (2014) Proteomic mapping of the human mitochondrial intermembrane space in live cells via ratiometric APEX tagging. *Mol Cell* **55**, 332-341
26. Bar, D. Z., Atkatsh, K., Tavarez, U., Erdos, M. R., Gruenbaum, Y., and Collins, F. S. (2018) Biotinylation by antibody recognition-a method for proximity labeling. *Nat Methods* **15**, 127-133
27. Pfaff, J., Rivera Monroy, J., Jamieson, C., Rajanala, K., Vilardi, F., Schwappach, B., and Kehlenbach, R. H. (2016) Emery-Dreifuss muscular dystrophy mutations impair TRC40-mediated targeting of emerin to the inner nuclear membrane. *J Cell Sci* **129**, 502-516
28. Chen, J., Zheng, X. F., Brown, E. J., and Schreiber, S. L. (1995) Identification of an 11-kDa FKBP12-rapamycin-binding domain within the 289-kDa FKBP12-rapamycin-associated protein and characterization of a critical serine residue. *Proc Natl Acad Sci U S A* **92**, 4947-4951
29. Cheng, L. C., Baboo, S., Lindsay, C., Brusman, L., Martinez-Bartolome, S., Tapia, O., Zhang, X., Yates, J. R., 3rd, and Gerace, L. (2019) Identification of new transmembrane proteins concentrated at the nuclear envelope using organellar proteomics of mesenchymal cells. *Nucleus* **10**, 126-143
30. Saiz-Ros, N., Czapiewski, R., Epifano, I., Stevenson, A., Swanson, S. K., Dixon, C. R., Zamora, D. B., McElwee, M., Vijayakrishnan, S., Richardson, C. A., Dong, L., Kelly, D. A., Pytowski, L., Goldberg, M. W., Florens, L., Graham, S. V., and Schirmer, E. C. (2019) Host Vesicle Fusion Protein VAPB Contributes to the Nuclear Egress Stage of Herpes Simplex Virus Type-1 (HSV-1) Replication. *Cells* **8,** doi: 10.3390/cells8020120
31. Cho, I. T., Adelmant, G., Lim, Y., Marto, J. A., Cho, G., and Golden, J. A. (2017) Ascorbate peroxidase proximity labeling coupled with biochemical fractionation identifies promoters of endoplasmic reticulum-mitochondrial contacts. *J Biol Chem* **292**, 16382-16392
32. Han, S., Udeshi, N. D., Deerinck, T. J., Svinkina, T., Ellisman, M. H., Carr, S. A., and Ting, A. Y. (2017) Proximity Biotinylation as a Method for Mapping Proteins Associated with mtDNA in Living Cells. *Cell Chem Biol* **24**, 404-414
33. Hung, V., Lam, S. S., Udeshi, N. D., Svinkina, T., Guzman, G., Mootha, V. K., Carr, S. A., and Ting, A. Y. (2017) Proteomic mapping of cytosol-facing outer mitochondrial and ER membranes in living human cells by proximity biotinylation. *Elife* **6,** doi: 10.7554/eLife.24463

34. Lee, S. Y., Kang, M. G., Park, J. S., Lee, G., Ting, A. Y., and Rhee, H. W. (2016) APEX Fingerprinting Reveals the Subcellular Localization of Proteins of Interest. *Cell Rep* **15**, 1837-1847
35. Paek, J., Kalocsay, M., Staus, D. P., Wingler, L., Pascolutti, R., Paulo, J. A., Gygi, S. P., and Kruse, A. C. (2017) Multidimensional Tracking of GPCR Signaling via Peroxidase-Catalyzed Proximity Labeling. *Cell* **169**, 338-349 e311
36. Bengtsson, L., and Otto, H. (2008) LUMA interacts with emerin and influences its distribution at the inner nuclear membrane. *J Cell Sci* **121**, 536-548
37. Liang, W. C., Mitsuhashi, H., Keduka, E., Nonaka, I., Noguchi, S., Nishino, I., and Hayashi, Y. K. (2011) TMEM43 mutations in Emery-Dreifuss muscular dystrophy-related myopathy. *Annals of Neurology* **69**, 1005-1013
38. Franke, W. W., Dorflinger, Y., Kuhn, C., Zimbelmann, R., Winter-Simanowski, S., Frey, N., and Heid, H. (2014) Protein LUMA is a cytoplasmic plaque constituent of various epithelial adherens junctions and composite junctions of myocardial intercalated disks: a unifying finding for cell biology and cardiology. *Cell Tissue Res* **357**, 159-172
39. Defeo-Jones, D., Huang, P. S., Jones, R. E., Haskell, K. M., Vuocolo, G. A., Hanobik, M. G., Huber, H. E., and Oliff, A. (1991) Cloning of cDNAs for cellular proteins that bind to the retinoblastoma gene product. *Nature* **352**, 251-254
40. Wu, M. Y., Eldin, K. W., and Beaudet, A. L. (2008) Identification of chromatin remodeling genes Arid4a and Arid4b as leukemia suppressor genes. *J Natl Cancer Inst* **100**, 1247-1259
41. Cartegni, L., di Barletta, M. R., Barresi, R., Squarzoni, S., Sabatelli, P., Maraldi, N., Mora, M., Di Blasi, C., Cornelio, F., Merlini, L., Villa, A., Cobianchi, F., and Toniolo, D. (1997) Heart-specific localization of emerin: new insights into Emery-Dreifuss muscular dystrophy. *Hum Mol Genet* **6**, 2257-2264
42. Salpingidou, G., Smertenko, A., Hausmanowa-Petrucewicz, I., Hussey, P. J., and Hutchison, C. J. (2007) A novel role for the nuclear membrane protein emerin in association of the centrosome to the outer nuclear membrane. *J Cell Biol* **178**, 897-904
43. Ohba, T., Schirmer, E. C., Nishimoto, T., and Gerace, L. (2004) Energy- and temperature-dependent transport of integral proteins to the inner nuclear membrane via the nuclear pore. *J Cell Biol.* **167**, 1051-1062.
44. Soullam, B., and Worman, H. J. (1995) Signals and structural features involved in integral membrane protein targeting to the inner nuclear membrane. *J Cell Biol* **130**, 15-27
45. Ungricht, R., Klann, M., Horvath, P., and Kutay, U. (2015) Diffusion and retention are major determinants of protein targeting to the inner nuclear membrane. *J Cell Biol* **209**, 687-704
46. Zuleger, N., Kelly, D. A., Richardson, A. C., Kerr, A. R., Goldberg, M. W., Goryachev, A. B., and Schirmer, E. C. (2011) System analysis shows distinct mechanisms and common principles of nuclear envelope protein dynamics. *J. Cell Biol.* **193**, 109-123.
47. Blenski, M., and Kehlenbach, R. H. (2019) Targeting of LRRC59 to the Endoplasmic Reticulum and the Inner Nuclear Membrane. *Int J Mol Sci* **20,** doi: 10.3390/ijms20020334.
48. Foisner, R., and Gerace, L. (1993) Integral membrane proteins of the nuclear envelope interact with lamins and chromosomes, and binding is modulated by mitotic phosphorylation. *Cell.* **73**, 1267-1279.
49. Furukawa, K., Pante, N., Aebi, U., and Gerace, L. (1995) Cloning of a cDNA for lamina-associated polypeptide 2 (LAP2) and identification of regions that specify targeting to the nuclear envelope. *EMBO J.* **14**, 1626-1636.
50. Sukegawa, J., and Blobel, G. (1993) A nuclear pore complex protein that contains zinc finger motifs, binds DNA, and faces the nucleoplasm. *Cell* **72**, 29-38
51. Cordes, V. C., Reidenbach, S., Rackwitz, H. R., and Franke, W. W. (1997) Identification of protein p270/Tpr as a constitutive component of the nuclear pore complex-attached intranuclear filaments. *J Cell Biol* **136**, 515-529

52. Rasala, B. A., Orjalo, A. V., Shen, Z., Briggs, S., and Forbes, D. J. (2006) ELYS is a dual nucleoporin/kinetochore protein required for nuclear pore assembly and proper cell division. *Proc Natl Acad Sci U S A* **103**, 17801-17806
53. Gerace, L., and Blobel, G. (1980) The nuclear envelope lamina is reversibly depolymerized during mitosis. *Cell* **19**, 277-287
54. Söderberg, O., Gullberg, M., Jarvius, M., Ridderstrale, K., Leuchowius, K. J., Jarvius, J., Wester, K., Hydbring, P., Bahram, F., Larsson, L. G., and Landegren, U. (2006) Direct observation of individual endogenous protein complexes in situ by proximity ligation. *Nat Methods* **3**, 995-1000
55. Chojnowski, A., Sobota, R. M., Ong, P. F., Xie, W., Wong, X., Dreesen, O., Burke, B., and Stewart, C. L. (2018) 2C-BioID: An Advanced Two Component BioID System for Precision Mapping of Protein Interactomes. *iScience* **10**, 40-52
56. Franz, C., Walczak, R., Yavuz, S., Santarella, R., Gentzel, M., Askjaer, P., Galy, V., Hetzer, M., Mattaj, I. W., and Antonin, W. (2007) MEL-28/ELYS is required for the recruitment of nucleoporins to chromatin and postmitotic nuclear pore complex assembly. *EMBO Rep* **8**, 165-172
57. Gillespie, P. J., Khoudoli, G. A., Stewart, G., Swedlow, J. R., and Blow, J. J. (2007) ELYS/MEL-28 chromatin association coordinates nuclear pore complex assembly and replication licensing. *Curr Biol* **17**, 1657-1662
58. Belshaw, P. J., Ho, S. N., Crabtree, G. R., and Schreiber, S. L. (1996) Controlling protein association and subcellular localization with a synthetic ligand that induces heterodimerization of proteins. *Proc Natl Acad Sci U S A* **93**, 4604-4607
59. Fasana, E., Fossati, M., Ruggiano, A., Brambillasca, S., Hoogenraad, C. C., Navone, F., Francolini, M., and Borgese, N. (2010) A VAPB mutant linked to amyotrophic lateral sclerosis generates a novel form of organized smooth endoplasmic reticulum. *FASEB J* **24**, 1419-1430
60. Gasteier, J. E., Madrid, R., Krautkramer, E., Schroder, S., Muranyi, W., Benichou, S., and Fackler, O. T. (2003) Activation of the Rac-binding partner FHOD1 induces actin stress fibers via a ROCK-dependent mechanism. *J Biol Chem* **278**, 38902-38912
61. Charneau, P., Mirambeau, G., Roux, P., Paulous, S., Buc, H., and Clavel, F. (1994) HIV-1 reverse transcription. A termination step at the center of the genome. *J Mol Biol* **241**, 651-662
62. Chen, C., and Okayama, H. (1987) High-efficiency transformation of mammalian cells by plasmid DNA. *Mol Cell Biol* **7**, 2745-2752
63. Atanassov, I., and Urlaub, H. (2013) Increased proteome coverage by combining PAGE and peptide isoelectric focusing: comparative study of gel-based separation approaches. *Proteomics* **13**, 2947-2955
64. Cox, J., and Mann, M. (2008) MaxQuant enables high peptide identification rates, individualized p.p.b.-range mass accuracies and proteome-wide protein quantification. *Nat Biotechnol* **26**, 1367-1372
65. Vizcaino, J. A., Deutsch, E. W., Wang, R., Csordas, A., Reisinger, F., Rios, D., Dianes, J. A., Sun, Z., Farrah, T., Bandeira, N., Binz, P. A., Xenarios, I., Eisenacher, M., Mayer, G., Gatto, L., Campos, A., Chalkley, R. J., Kraus, H. J., Albar, J. P., Martinez-Bartolome, S., Apweiler, R., Omenn, G. S., Martens, L., Jones, A. R., and Hermjakob, H. (2014) ProteomeXchange provides globally coordinated proteomics data submission and dissemination. *Nat Biotechnol* **32**, 223-226
66. Carpenter, A. E., Jones, T. R., Lamprecht, M. R., Clarke, C., Kang, I. H., Friman, O., Guertin, D. A., Chang, J. H., Lindquist, R. A., Moffat, J., Golland, P., and Sabatini, D. M. (2006) CellProfiler: image analysis software for identifying and quantifying cell phenotypes. *Genome Biol* **7**, R100

Figure legends

Figure 1
VAPB localizes to the INM.
(A) HeLa cells were grown on coverslips and subjected to indirect immunofluorescence using antibodies against VAPB. Cells were blocked (i) with 3% BSA or (ii) with Sigma Duolink blocking solution.
(B) HeLa cells were transfected with plasmids coding for mCherry-FRB-VAPB or HA-FRB-VAPB, as indicated.
(C) HeLa cells were co-transfected with plasmids coding for mCherry-FRB-VAPB and dGFP-GST-cNLS-FKBP12. After treatment with (+) or without (-) rapamycin, cells were fixed and analyzed by confocal microscopy. Scale bar, 10 µm.
(D) HeLa cells were analysed by immunoelectron microscopy, using antibodies against VAPB. C, cytoplasm; M, mitochondria; N, nucleus. The arrows indicate nuclear pore complexes. Scale bar, 100 nm.

Figure 2
Comparison of the classic and a new APEX-approach.
(A) Schemes of the "direct fusion (classic) approach" (left) and the "rapamycin (new) approach" (right).
(B) For the direct fusion and the rapamycin approach, cells were transfected with plasmids coding for GFP-APEX2 or APEX2-VAPB and FKBP12-GFP-APEX2 and mCherry-FRB-VAPB, respectively. Cells were analyzed directly (left) or upon incubation with or without rapamycin (right). Scale bar, 10 µm.
(C) Cells were transfected as in B and subjected to the biotinylation protocol. Biotinylated proteins were enriched using neutravidin beads and total and bound proteins were analyzed by SDS-PAGE followed by Western blotting. Note that GFP-APEX2 (lanes 5 and 7) and APEX2-VAPB (lanes 6 and 8) have very similar molecular weights.

Figure 3
Proximity mapping of mCherry-FRB-VAPB by RAPIDS.
(A) Experimental workflow. Cells grown in "light" or "heavy" medium are co-transfected with plasmids coding for FKBP12-GFP-APEX2 and mCherry-FRB-VAPB, and subjected to APEX2-dependent biotinylation in the absence or presence of rapamycin. Note that this labelling scheme reflects the reverse reaction. In the forward reaction, "light" and "heavy" media are used for cells treated with or without rapamycin, respectively. Proteins from cell lysates are bound to neutravidin beads and the total and the bound fractions are analyzed by LC-MS.
(B) The scatter plot resulting from two independent experiments shows normalized $\log_2$-ratios of proteins eluted from neutravidin beads in forward (heavy medium (H), without rapamycin; light (L) medium, with rapamycin; x-axis) and reverse (heavy medium (H), with rapamycin; light (L) medium, without rapamycin y-axis) experiments. The plot focuses on the upper left quadrant, because in the forward reaction, low H/L-ratios (i.e. negative $\log_2$-values) are expected for specific hits, whereas high ratios are expected in the reverse reaction. Known interacting partners of VAPB are underlined. Closed circles: proteins that were significant in all experiments; open triangles: proteins that were significant only in forward experiments; open squares: proteins that were significant only in reverse experiments.
(C) Total cell lysates (total) and proteins bound to neutravidin beads (bound) from one of the experiments depicted in (B) were analyzed by Western blotting, using antibodies against VAPB, ACBD5, OSBPL9 and emerin and GAPDH as a loading control.

Figure 4
RAPIDS using HA-FRB-VAPB.
(A) Experimental workflow. Cells are grown in "light" or "heavy" medium as indicated, co-transfected with plasmids coding for APEX2-dGFP-cNLS-FKBP12 and HA-FRB-VAPB, and subjected to RAPIDS as described in Fig. 3A.

(B) Transfected cells were treated with or without rapamycin as indicated, fixed and analyzed by fluorescence microscopy. Scale bar, 10 µm.
(C) The scatter plot resulting from two independent experiments shows normalized log_2-ratios of proteins eluted from neutravidin beads in forward (heavy medium (H), without rapamycin; light (L) medium, with rapamycin; x-axis) and reverse (heavy medium (H), with rapamycin; light (L) medium, without rapamycin y-axis) experiments. As in Fig. 3, the plot focuses on the upper left quadrant. Closed circles: proteins that were significant in all experiments; open triangles: proteins that were significant only in forward experiments; open squares: proteins that were significant only in reverse experiments.
(D) Total cell lysates (total) and proteins bound to neutravidin beads (bound) from experiments depicted in (C) were analyzed by Western blotting using antibodies against VAPB, ELYS, Lamin B1, Nup153, Lamin A/C, TMPO, TOR1AIP1, SEC22b, emerin and GAPDH as a loading control.

Figure 5
VAPB forms complexes with emerin, TMEM43 and ELYS.
(A) HeLa cells were treated with (+) or without (-; DMSO as a control) DSP and endogenous proteins from cell lysates were precipitated using rabbit-anti-VAPB and rabbit IgG as a control. *, IgG heavy chain.
(B) HeLa cells were transfected with constructs coding for HA-FRB-VAPB or HA-FRB and subjected to crosslinking with (+) or without (-; DMSO as a control) DSP. Proteins from cell-lysates were immunoprecipitated using anti-HA antibodies. Note that HA-FRB was expressed and precipitated to similar levels as HA-FRB-VAPBB (data not shown). (A, B) Precipitated proteins were analyzed by Western blotting, detecting VAPB, ACBD5, OSBPL9, emerin, TMEM43, ELYS, the HA-tag and, for control, Na^+/K^+-ATPase, as indicated.

Figure 6
VAPB is in close proximity to emerin and ELYS.
(A, B) Cells were treated with siRNAs against VAPB or non-targeting (nt) siRNAs as indicated and subjected to PLAs using antibodies against VAPB (A and B) and emerin (A) or ELYS (B), respectively. Indirect immunofluorescence was used to detect VAPB. The graphs show the quantification of PLA-results from three independent experiments, analyzing a total of 450 cells. The bars indicate mean values ± SD. Single antibody controls were performed to confirm the specificity of PLA interactions. ***, $P<0.001$. Scale bars, 10 µm.

Figure 7
The VAPB-interactome. Schematic representation of the protein network identified by RAPIDS using HA-FRB-VAPB (HA-VAPB) with APEX2-dGFP-cNLS-FKBP12 (NLS-APEX2) or mCherry-FRB-VAPB (mCherry-VAPB) with FKBP12-GFP-APEX2 (APEX2). Dotted lines indicate interactions that have also been found in previous studies.

Figure 1

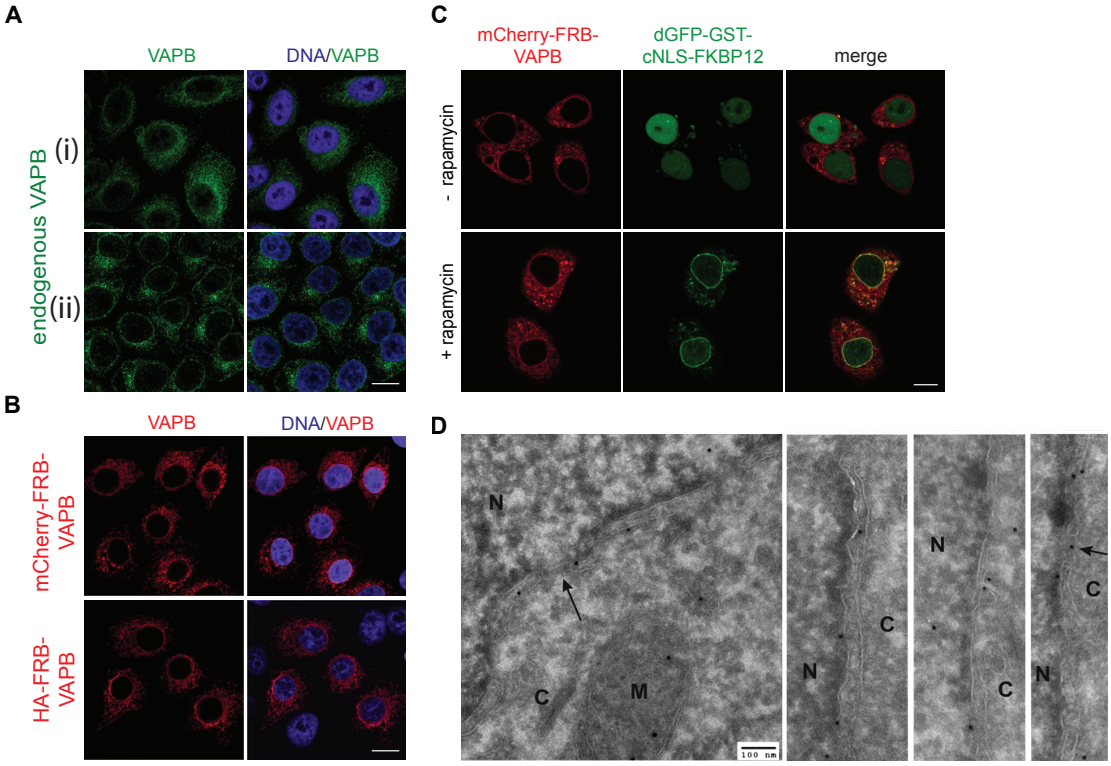
A
VAPB
DNA/VAPB
endogenous VAPB
(i)
(ii)
B
VAPB
DNA/VAPB
mCherry-FRB-VAPB
HA-FRB-VAPB
C
mCherry-FRB-VAPB
dGFP-GST-cNLS-FKBP12
merge
- rapamycin
+ rapamycin
D
N
C
M
100 nm

Figure 2

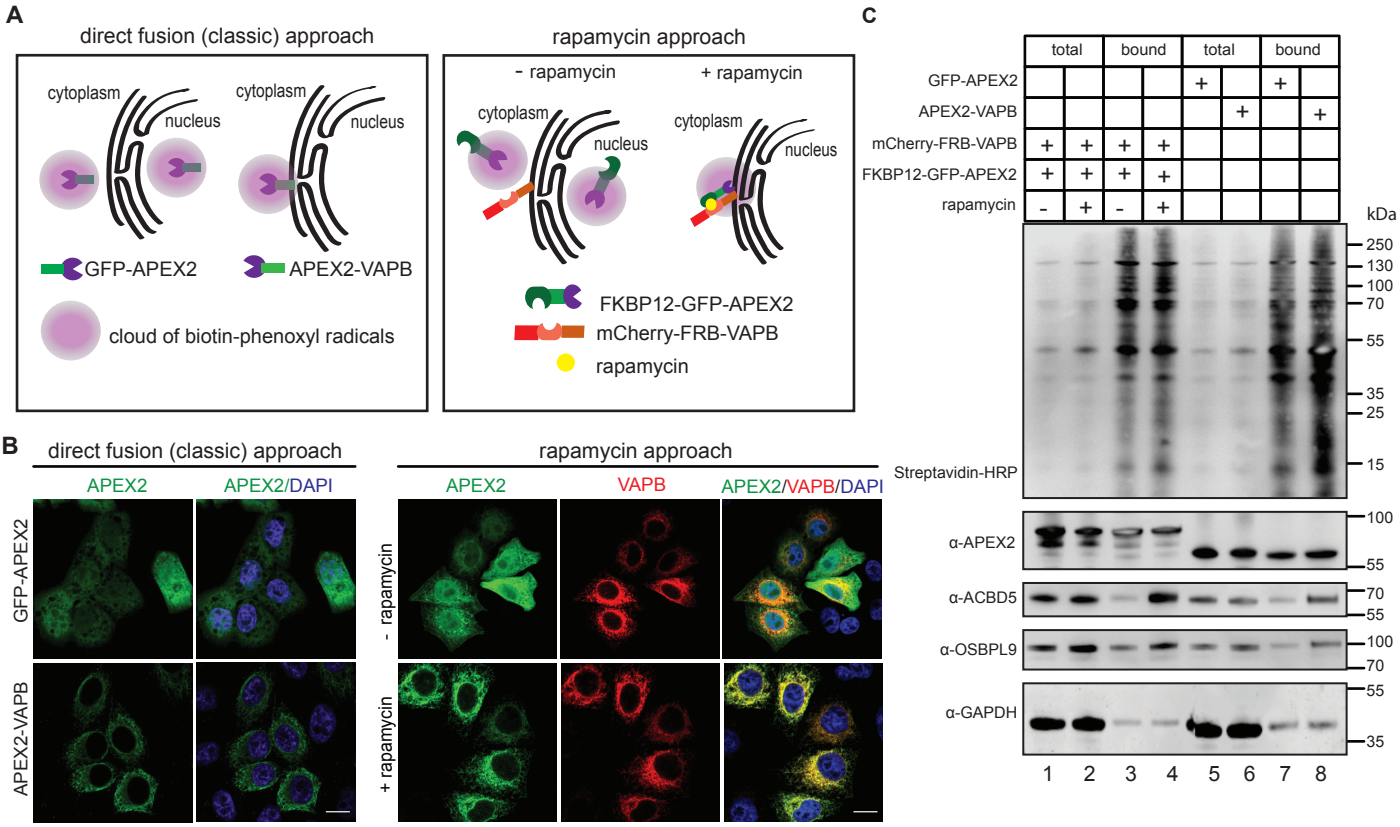
A
direct fusion (classic) approach
rapamycin approach
- rapamycin
+ rapamycin
cytoplasm
nucleus
GFP-APEX2
APEX2-VAPB
cloud of biotin-phenoxyl radicals
FKBP12-GFP-APEX2
mCherry-FRB-VAPB
rapamycin
B
direct fusion (classic) approach
rapamycin approach
APEX2
APEX2/DAPI
VAPB
APEX2/VAPB/DAPI
GFP-APEX2
APEX2-VAPB
- rapamycin
+ rapamycin
C
total
bound
GFP-APEX2
APEX2-VAPB
mCherry-FRB-VAPB
FKBP12-GFP-APEX2
rapamycin
kDa
250
130
100
70
55
35
25
15
Streptavidin-HRP
α-APEX2
α-ACBD5
α-OSBPL9
α-GAPDH
1 2 3 4 5 6 7 8

Figure 3

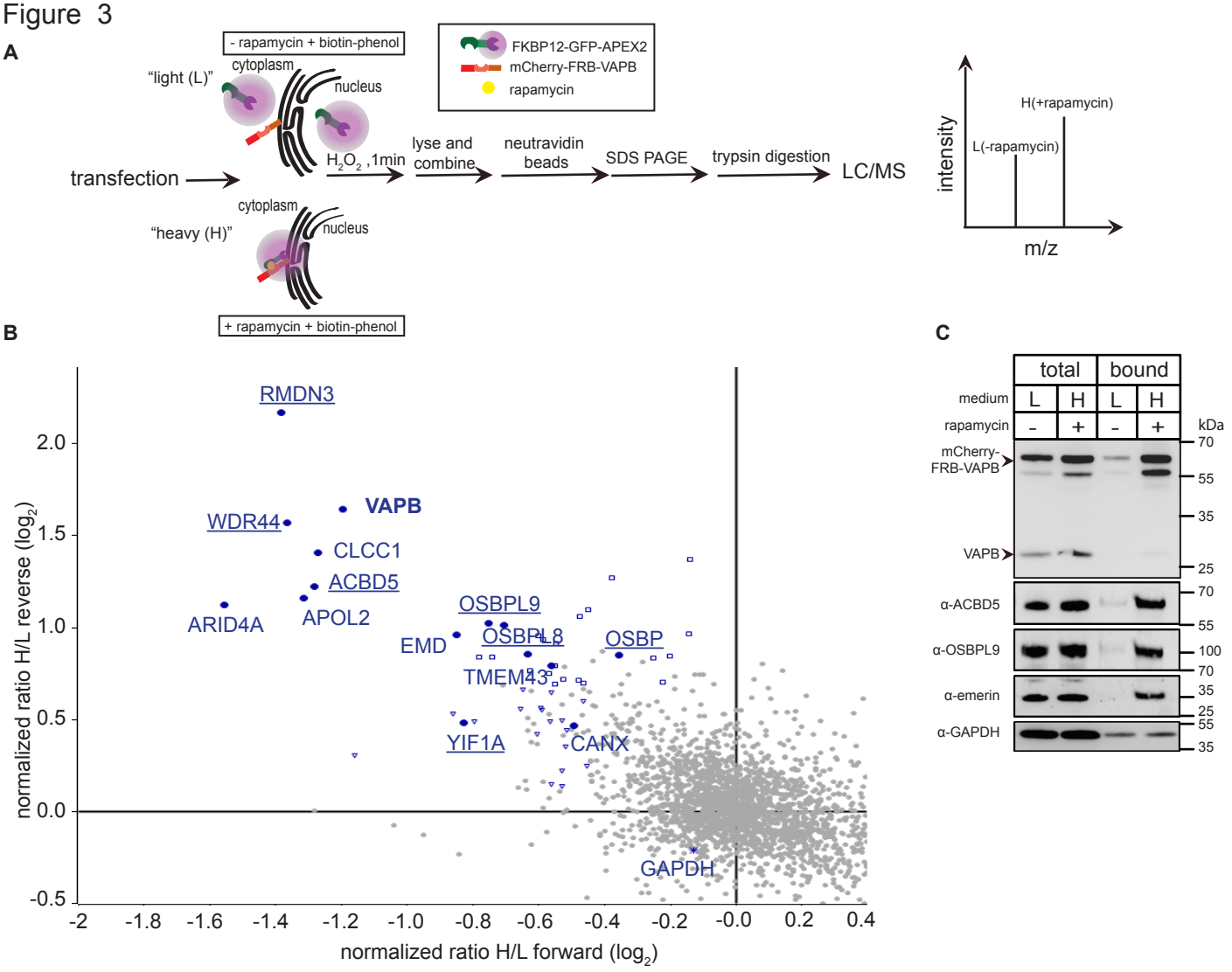
A
- rapamycin + biotin-phenol
FKBP12-GFP-APEX2
mCherry-FRB-VAPB
rapamycin
"light (L)"
cytoplasm
nucleus
transfection
H_2O_2 ,1min
lyse and combine
neutravidin beads
SDS PAGE
trypsin digestion
LC/MS
"heavy (H)"
+ rapamycin + biotin-phenol
intensity
H(+rapamycin)
L(-rapamycin)
m/z
B
RMDN3
VAPB
WDR44
CLCC1
ACBD5
ARID4A
APOL2
OSBPL9
EMD
OSBPL8
OSBP
TMEM43
YIF1A
CANX
GAPDH
normalized ratio H/L reverse (log_2)
normalized ratio H/L forward (log_2)
C
total
bound
medium
L
H
rapamycin
kDa
mCherry-FRB-VAPB
VAPB
α-ACBD5
α-OSBPL9
α-emerin
α-GAPDH

Figure 4

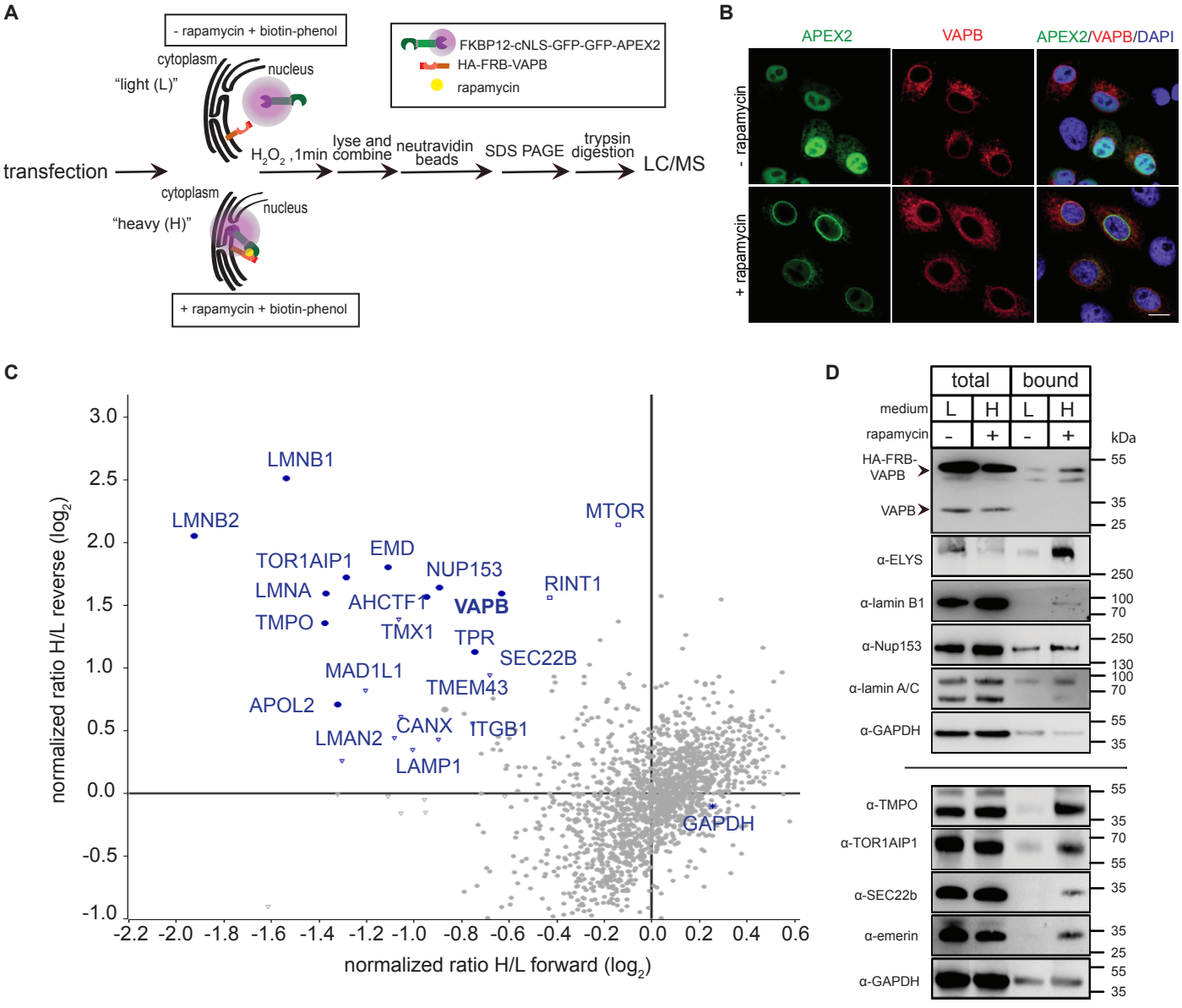
A
- rapamycin + biotin-phenol
cytoplasm
nucleus
"light (L)"
FKBP12-cNLS-GFP-GFP-APEX2
HA-FRB-VAPB
rapamycin
transfection
H2O2 ,1min
lyse and combine
neutravidin beads
SDS PAGE
trypsin digestion
LC/MS
cytoplasm
nucleus
"heavy (H)"
+ rapamycin + biotin-phenol
B
APEX2
VAPB
APEX2/VAPB/DAPI
- rapamycin
+ rapamycin
C
normalized ratio H/L reverse (log2)
normalized ratio H/L forward (log2)
LMNB1
LMNB2
MTOR
TOR1AIP1
EMD
NUP153
RINT1
LMNA
AHCTF1
VAPB
TMPO
TMX1
TPR
SEC22B
MAD1L1
TMEM43
APOL2
CANX
ITGB1
LMAN2
LAMP1
GAPDH
D
total
bound
medium
L
H
L
H
rapamycin
-
+
-
+
kDa
HA-FRB-VAPB
VAPB
α-ELYS
α-lamin B1
α-Nup153
α-lamin A/C
α-GAPDH
α-TMPO
α-TOR1AIP1
α-SEC22b
α-emerin
α-GAPDH

Figure 5

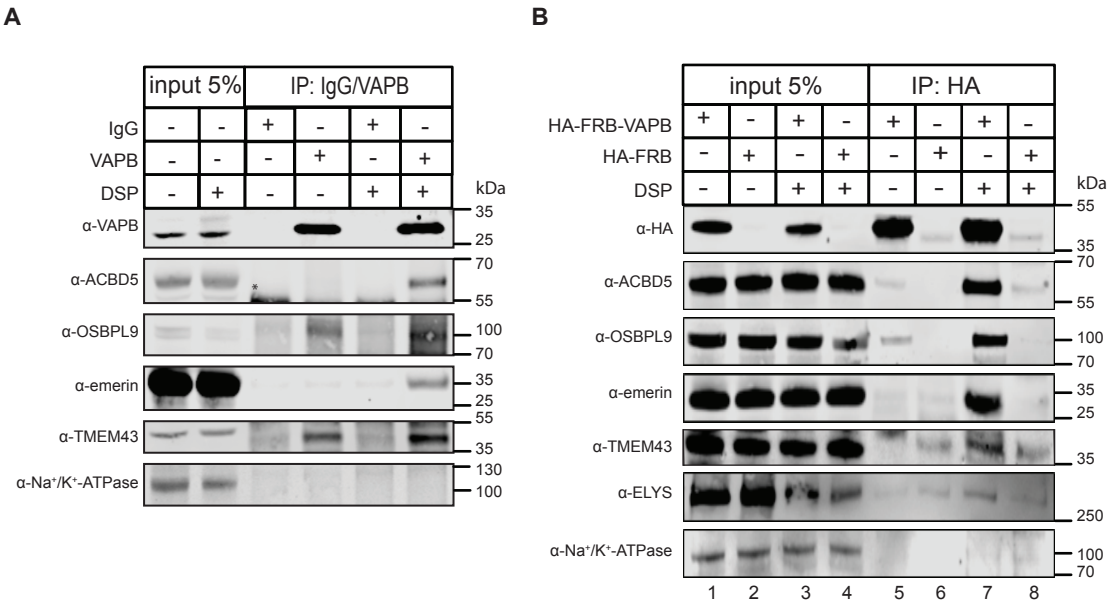
A
input 5%
IP: IgG/VAPB
IgG
VAPB
DSP
kDa
α-VAPB
α-ACBD5
α-OSBPL9
α-emerin
α-TMEM43
α-Na⁺/K⁺-ATPase
B
input 5%
IP: HA
HA-FRB-VAPB
HA-FRB
DSP
kDa
α-HA
α-ACBD5
α-OSBPL9
α-emerin
α-TMEM43
α-ELYS
α-Na⁺/K⁺-ATPase
1 2 3 4 5 6 7 8

Figure 6

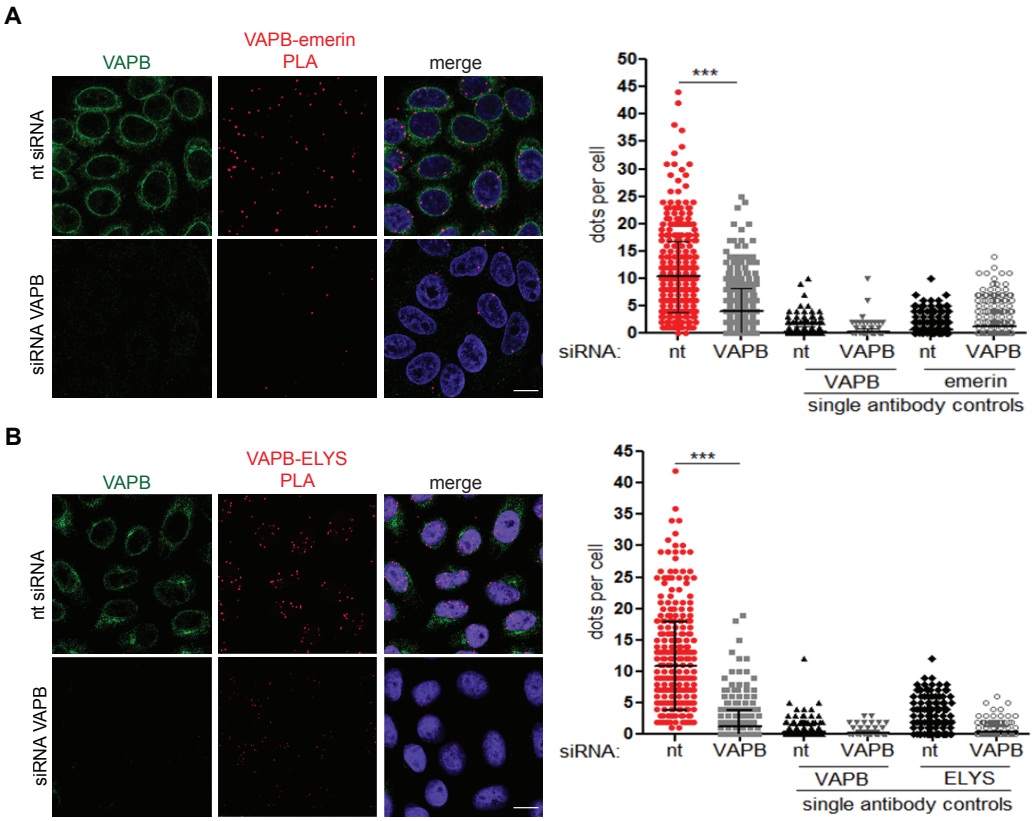
A
VAPB
VAPB-emerin PLA
merge
nt siRNA
siRNA VAPB
dots per cell
***
siRNA:
nt
VAPB
nt
VAPB
nt
VAPB
VAPB
emerin
single antibody controls
B
VAPB
VAPB-ELYS PLA
merge
nt siRNA
siRNA VAPB
dots per cell
***
siRNA:
nt
VAPB
nt
VAPB
nt
VAPB
VAPB
ELYS
single antibody controls

Figure 7

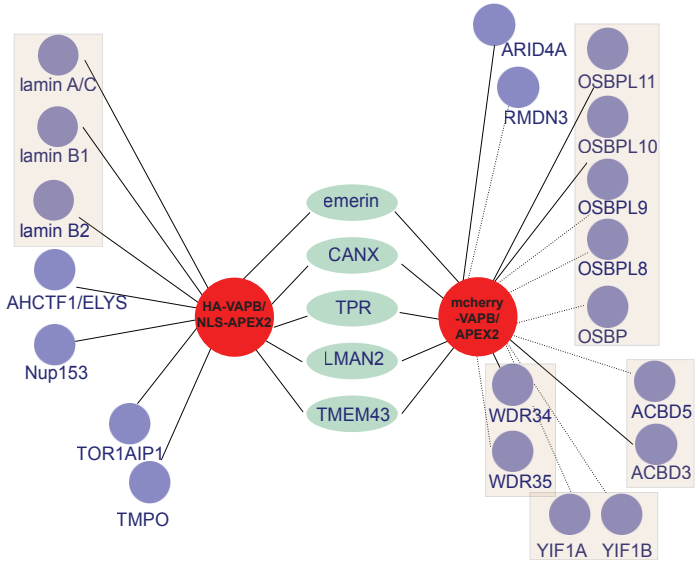
lamin A/C
lamin B1
lamin B2
AHCTF1/ELYS
Nup153
TOR1AIP1
TMPO
HA-VAPB/
NLS-APEX2
emerin
CANX
TPR
LMAN2
TMEM43
mcherry
-VAPB/
APEX2
ARID4A
RMDN3
OSBPL11
OSBPL10
OSBPL9
OSBPL8
OSBP
WDR34
WDR35
ACBD5
ACBD3
YIF1A
YIF1B

Proteomic mapping by rapamycin-dependent targeting of APEX2 identifies binding partners of VAPB at the inner nuclear membrane

Christina James, Marret Müller, Martin W. Goldberg, Christof Lenz, Henning Urlaub and Ralph H. Kehlenbach

J. Biol. Chem. published online September 13, 2019

Access the most updated version of this article at doi: 10.1074/jbc.RA118.007283